

Metal–insulator transition in $\text{Nd}_{1-x}\text{Eu}_x\text{NiO}_3$ compounds

This article has been downloaded from IOPscience. Please scroll down to see the full text article.

2006 J. Phys.: Condens. Matter 18 6117

(<http://iopscience.iop.org/0953-8984/18/26/030>)

View [the table of contents for this issue](#), or go to the [journal homepage](#) for more

Download details:

IP Address: 129.252.86.83

The article was downloaded on 28/05/2010 at 12:01

Please note that [terms and conditions apply](#).

Metal–insulator transition in $\text{Nd}_{1-x}\text{Eu}_x\text{NiO}_3$ compounds

M T Escote¹, V B Barbeta², R F Jardim³ and J Campo⁴

¹ Instituto de Química, Universidade Estadual de São Paulo, Campus Araraquara, CP 353, 14801-970, Araraquara, SP, Brazil

² Departamento de Física, Centro Universitário da FEI, Av. Humberto de A. C. Branco 3972, 09850-901, S. B. Campo, SP, Brazil

³ Instituto de Física, Universidade de São Paulo, CP 66318, 05315-970, São Paulo, SP, Brazil

⁴ Instituto de Ciencia de Materiales de Aragón, Facultad de Ciencias, Universidad de Zaragoza, C/Pedro Cerbuna 12, 50009 Zaragoza, Spain

E-mail: rjardim@if.usp.br

Received 2 January 2006, in final form 13 May 2006

Published 19 June 2006

Online at stacks.iop.org/JPhysCM/18/6117

Abstract

Polycrystalline $\text{Nd}_{1-x}\text{Eu}_x\text{NiO}_3$ ($0 \leq x \leq 0.5$) compounds were synthesized in order to investigate the character of the metal–insulator (MI) phase transition in this series. Samples were prepared through the sol–gel route and subjected to heat treatments at $\sim 1000^\circ\text{C}$ under oxygen pressures as high as 80 bar. X-ray diffraction (XRD) and neutron powder diffraction (NPD), electrical resistivity $\rho(T)$, and magnetization $M(T)$ measurements were performed on these compounds. The NPD and XRD results indicated that the samples crystallize in an orthorhombic distorted perovskite structure, space group $Pbnm$. The analysis of the structural parameters revealed a sudden and small expansion of $\sim 0.2\%$ of the unit cell volume when electronic localization occurs. This expansion was attributed to a small increase of $\sim 0.003 \text{ \AA}$ of the average Ni–O distance and a simultaneous decrease of $\sim -0.5^\circ$ of the Ni–O–Ni superexchange angle. The $\rho(T)$ measurements revealed a MI transition occurring at temperatures ranging from $T_{\text{MI}} \sim 193$ to 336 K for samples with $x = 0$ and 0.50, respectively. These measurements also show a large thermal hysteresis in NdNiO_3 during heating and cooling processes, suggesting a first-order character of the phase transition at T_{MI} . The width of this thermal hysteresis was found to decrease appreciably for the sample $\text{Nd}_{0.7}\text{Eu}_{0.3}\text{NiO}_3$. The results indicate that cation disorder associated with increasing substitution of Nd by Eu is responsible for changing the first-order character of the transition in NdNiO_3 .

1. Introduction

Since the discovery of high- T_c superconductivity in copper oxides a great interest has been renewed in transition-metal oxide systems [1]. The perovskites with general formula $RNiO_3$ ($R =$ rare earth) are typical examples which have been investigated due to their interesting transport and magnetic properties [2–15]. Moreover, these compounds provide a remarkable opportunity to study the relationship between structural changes and physical properties in perovskite-like oxides [6, 11, 14]. Perhaps the most interesting property of these series is the occurrence of a temperature-driven metal–insulator (MI) transition in compounds with $R \neq$ La [2–4]. In fact, electrical resistivity measurements performed on polycrystalline and thin films of $LaNiO_3$ revealed a metal-like behaviour down to 1.5 K [3, 15]. However, in other members of this family, such as $PrNiO_3$ and $NdNiO_3$, a very sharp MI transition is frequently verified [3]. The temperature T_{MI} , in which the MI transition occurs, has been found to increase systematically as the size of the rare-earth ion decreases, being 130 K for $PrNiO_3$ and reaching values as high as 480 K in $EuNiO_3$ [3]. These compounds crystallize, in the itinerant-electron phase, in an orthorhombically distorted perovskite structure (space group $Pbnm$). A higher distortion of the perovskite structure is often observed when the rare-earth ion size is decreased due to the tilt of the NiO_6 octahedra and a consequent reduction of the superexchange Ni–O–Ni angle [2]. These observed features seem to indicate that the MI transition is closely related to both the degree of distortion of the ideal perovskite structure and the Ni–O–Ni bond angle [5, 6].

High-resolution neutron powder diffraction (NPD) experiments performed on $PrNiO_3$, $NdNiO_3$, and $SmNiO_3$ compounds have revealed that the MI transition is accompanied by a small structural change in the unit cells [6]. The data also indicate that the unit cell volume undergoes a subtle increase when the system evolves toward the insulator regime due to a slight increase in the average Ni–O distance [6]. This effect induces additional tilts of the NiO_6 octahedra, which also implies a subtle decrease of the Ni–O–Ni bond angle.

Some recent results in smaller rare-earth ions ($R =$ Ho, Y, Er and Lu) suggested a change in the crystal symmetry, from orthorhombic $Pbnm$ to monoclinic $P2_1/n$, when the system evolves from the metallic to the insulating state, due to a charge disproportionation of Ni^{3+} cations [13]. Results of electron diffraction and Raman scattering indicated a symmetry break also for $NdNiO_3$ [16]. A direct observation of charge order in epitaxial $NdNiO_3$ films, using resonant x-ray scattering, was also reported [17]. These results have led to the proposition that charge disproportionation and the structural phase transition from orthorhombic $Pbnm$ to monoclinic $P2_1/n$ should occur for all the rare-earth family at T_{MI} , although it would be difficult to discriminate the two types of Ni site. This charge-ordered state would also explain the unusual propagation vector observed in neutron experiments, and it would make models with orbital order obsolete [17]. On the other hand, Mössbauer spectroscopy measurements in the $Nd_{0.98}Fe_{0.02}NiO_3$ compound, performed by Presniakov *et al* [18], have showed the existence of only one Ni chemical specimen, indicating that there is no charge disproportionation in the insulating phase and, therefore, there is no change in the lattice symmetry for this compound at T_{MI} .

Concerning the magnetic properties of these nickelates, muon-spin relaxation experiments carried out on $RNiO_3$ perovskites ($R =$ Pr, Nd, Sm, Eu) [3] have revealed the occurrence of an antiferromagnetic ordering of the Ni^{3+} sublattice. For Pr and Nd compounds, the magnetic ordering occurs at temperatures T_N close to T_{MI} , whereas other members of this family display $T_N < T_{MI}$. Such a behaviour has been confirmed by neutron powder diffraction experiments [19]. The magnetic ordering of the Ni sublattice exhibits an unusual antiferromagnetic order [20] that has been interpreted as the result of a spin density wave

(SDW) phase [11]. Furthermore, a combination of transport and thermal characterizations has suggested that the character of the MI transition is of first order in compounds that display $T_N \sim T_{\text{MI}}$, and of second order for compounds with $T_N < T_{\text{MI}}$ [21]. In fact, high-resolution PES photoemission measurements by Vobornik *et al* [9] have revealed two different electronic regimes for the RNiO_3 compounds with $T_N \sim T_{\text{MI}}$ and $T_N < T_{\text{MI}}$. However, a more profound discussion regarding this point requires consideration about the mechanism responsible for the MI transition, which is still a point of controversy in these nickelates. In fact, a complete understanding of the MI transition in this series certainly requires extra experimental data.

Within this scenario, this work focuses on the preparation and characterization of polycrystalline samples of $\text{Nd}_{1-x}\text{Eu}_x\text{NiO}_3$ ($0 \leq x \leq 0.5$). The interrelations between the structural and physical properties of these compounds have been studied. The results have enabled the discussion of the changes observed in compounds where the antiferromagnetic ordering occurs essentially at the same temperature $T_N \sim 200$ K but the MI transition varies systematically from ~ 193 to 336 K. In addition, the change of the character of the MI transition is discussed within the framework of the critical phenomena scenario from first to second order when the Eu content is increased.

2. Experimental procedure

2.1. Sample preparation

Polycrystalline samples of $\text{Nd}_{1-x}\text{Eu}_x\text{NiO}_3$ ($0 \leq x \leq 0.5$) were prepared by using sol–gel precursors, sintered at high temperatures (~ 1000 °C), and under oxygen pressures up to 80 bar. Details of the route employed and the sintering process for preparing these samples are given elsewhere [22]. Samples of NdAlO_3 and EuAlO_3 were also prepared in order to subtract the contribution to the magnetic susceptibility $\chi(T)$ arising from the $\text{Nd}_{1-x}\text{Eu}_x$ -ions. These samples were produced by mixing appropriate amounts of Nd_2O_3 , Eu_2O_3 , and Al_2O_3 . The intimate mixtures were sintered at ~ 1400 °C in air for ~ 100 h.

2.2. Sample characterization

All samples were characterized by means of x-ray diffraction (XRD) measurements in a Bruker D8 Advanced diffractometer using $\text{Cu K}\alpha$ radiation ($\lambda = 1.54056$ Å). Typical 2θ angular scans ranging between 20° and 100° , in steps of 0.02° , and accumulation time ~ 10 s were used in these experiments. Data were collected at room temperature (RT) and MgO was used as an internal standard. The cell parameters were calculated from the corrected peak positions for all identified reflections between $20^\circ \leq 2\theta \leq 100^\circ$.

Structural characterizations were also made by means of neutron powder diffraction (NPD) measurements on two selected samples: NdNiO_3 and $\text{Nd}_{0.7}\text{Eu}_{0.3}\text{NiO}_3$. The experiments were performed in the high-flux and medium-resolution D20 diffractometer at the Institut Laue-Langevin (Grenoble). The D20 instrument is equipped with a PSD-detector spanning an angular range from 1° to 160° (2θ) with a wavelength $\lambda = 1.2989$ Å (Cu(200) monochromator). An ‘orange’ cryostat was used for the measurements performed at low temperatures. The data were taken after first cooling the sample from RT down to ~ 50 K. Then the sample was warmed up (10 min K^{-1}) and the NPD data were collected at several temperatures up to 320 K. The accumulation time per spectrum was 10 min and the temperature stability is estimated as being close to 0.5 K. In order to minimize the neutron absorption by Eu, the $\text{Nd}_{0.7}\text{Eu}_{0.3}\text{NiO}_3$ sample was placed in a hollow vanadium can.

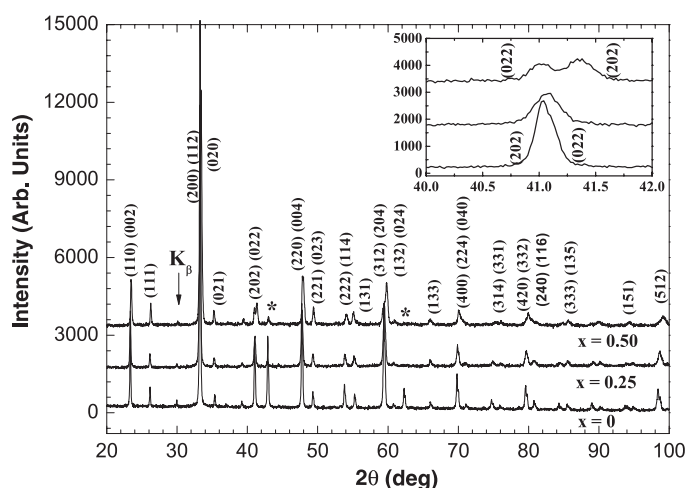


Figure 1. XRD patterns obtained at RT for $\text{Nd}_{1-x}\text{Eu}_x\text{NiO}_3$, $x = 0, 0.25$, and 0.50 . The inset displays the evolution of the peaks (022) and (202) for increasing Eu content. The symbol ‘*’ indicates the peaks corresponding to the MgO internal standard.

All the diffraction patterns were analysed by the Rietveld method using the FullProf program [23]. The data for $2\theta > 100^\circ$ were excluded in the refinements due to the low resolution of the D20 diffractometer in this angular range.

The temperature dependence of the electrical resistivity $\rho(T)$ was measured by the standard dc four-probe method in the temperature range from 77 to 400 K. Four copper electrical leads were attached with Ag epoxy to gold film contact pads on bar shaped samples, and the sample temperature was measured using a Pt thermometer. The temperature T_{MI} , in which the metal–insulator transition occurs, was defined as the temperature of the maximum in the $(1/\rho)(d\rho/dT)$ against T curves taken upon heating.

Magnetization $M(T)$ measurements were taken in a commercial MPMS superconducting quantum interference device (SQUID) magnetometer from Quantum Design. Zero-field-cooled (ZFC) and field-cooled (FC) runs were performed, with the temperature ranging from 5 to 400 K and under dc magnetic fields as high as 10 kOe.

3. Results and discussion

3.1. Crystal structure

Figure 1 displays some of the XRD patterns of $\text{Nd}_{1-x}\text{Eu}_x\text{NiO}_3$ compounds obtained at RT. The data showed no extra reflections belonging to impurity phases. In addition, the systematic observation of the peak related to the K_β radiation for the most intense reflection occurring close to $2\theta \sim 30^\circ$ strongly indicates that the samples have a high degree of crystallinity.

All peaks of the x-ray patterns were indexed with the orthorhombic distorted perovskite structure, space group $Pbnm$ [24]. In this crystal structure, atoms are placed at the following Wyckoff positions: R (R = Nd or Eu) and O(1) at $4c (x, y, 1/4)$; Ni at $4b (1/2, 0, 0)$; and O(2) at $8d (x, y, z)$. The actual Nd substitution by Eu was inferred, for instance, by the systematic changes observed in the (022) and (202) peaks with increasing Eu content, as displayed in the inset of figure 1. The data first reveal a systematic shift of the reflections to higher 2θ values,

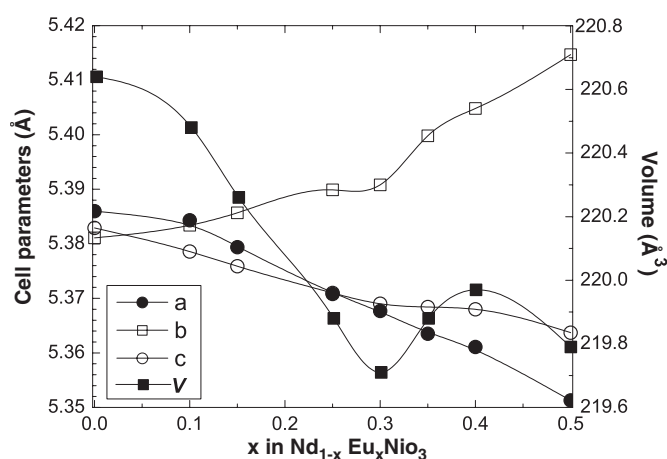


Figure 2. Room temperature cell parameters a , b , and c , and unit cell volume V of polycrystalline samples of $\text{Nd}_{1-x}\text{Eu}_x\text{NiO}_3$, as a function of Eu content x , obtained through XRD data.

as expected for a substitution of Nd by the smaller Eu ion. In addition, the separation of the peaks is hardly seen for samples with $x = 0$ and 0.25, but there is a clear broadening. For the sample with $x = 0.50$, both (022) and (202) peaks are well separated in 2θ .

Structural refinements were performed in all diagrams by using as starting parameters those reported in the literature for both NdNiO_3 and EuNiO_3 compounds [6, 25]. The refined cell parameters (a , b , and c), the unit cell volume (V), and the atomic positions were found to be in agreement with those expected for $\text{Nd}_{1-x}\text{Eu}_x\text{NiO}_3$ samples ($0 \leq x \leq 0.5$), i.e., the structural parameters were between those of NdNiO_3 and EuNiO_3 compounds. The resulting values of a , b , c , and V are plotted as a function of Eu concentration in figure 2. As a general trend, V , and the cell parameters a and c , decrease as the Eu content evolves, and an increase of the cell parameter b is observed. This is the expected behaviour due to the smaller size of the Eu ion compared to the Nd ion. For $x \approx 0.30$, a change in the volume V of the unit cell takes place and is certainly related to the occurrence of the MI transition at RT.

In order to study the thermal evolution of the crystal structure, characterizations through NPD as a function of temperature were carried out on two selected samples: NdNiO_3 and $\text{Nd}_{0.7}\text{Eu}_{0.3}\text{NiO}_3$. An initial analysis of the NPD patterns of both samples at RT revealed that the materials were stoichiometric and single phase, as inferred from the absence of peaks belonging to extra phases. These results agree with the analysis performed previously through XRD.

All NPD diagrams were also analysed through Rietveld refinements. First, the RT patterns of $\text{Nd}_{1-x}\text{Eu}_x\text{NiO}_3$ samples were analysed and then the sequential FullProf program was used for all other temperatures. In these refinements, the starting structural parameters were those listed for NdNiO_3 [2].

A typical example of one of these refinements is shown in figure 3 that exhibits the NPD pattern for the sample of NdNiO_3 at $T = 300$ K and the one calculated. This figure displays all the reflections belonging to the desired phase which were indexed on the basis of the orthorhombic GdFeO_3 -type perovskite [2]. The excellent quality of the fitting was confirmed by the R_{Bragg} reliability factor of ~ 3 , as displayed in table 1. This table also contains the refined atomic positions, cell parameters, B -factors (thermal motion parameters), the average Ni–O and R–O distances, and the superexchange angle θ along with reliability factors for both samples at three selected temperatures.

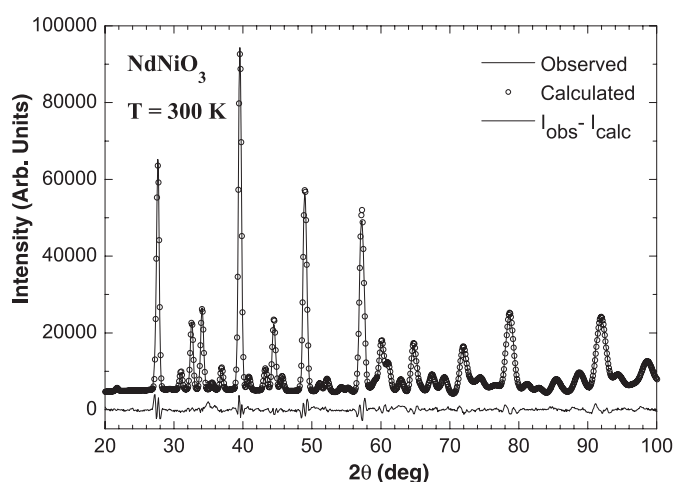


Figure 3. Observed (open circles), calculated (solid line), and the difference profile (bottom line) of the room temperature NPD pattern for the NdNiO_3 sample.

The NPD results at RT for the NdNiO_3 sample are in excellent agreement with those previously reported for the same compound [6]. For the Eu-substituted sample the results are adequate, since they would be associated with a material having cell parameters between those observed in NdNiO_3 and EuNiO_3 compounds [6, 25]. The R_{Bragg} values for the $\text{Nd}_{0.7}\text{Eu}_{0.3}\text{NiO}_3$ patterns, taken at several temperatures, were greater than those for the unsubstituted sample. Nevertheless, it is worth mentioning that excellent Rietveld refinements in all NPD diagrams were obtained by adopting the orthorhombic GdFeO_3 -type perovskite. Obviously, due to the increasing disorder related to the partial substitution of Nd by Eu, the reliability factors R_{Bragg} for the Eu-substituted sample were greater than those for the NdNiO_3 compound. However, the values of R_{Bragg} between 5 and 6 in $\text{Nd}_{0.7}\text{Eu}_{0.3}\text{NiO}_3$ are similar to the ones obtained for the NdNiO_3 compound elsewhere [6].

From figures 4 and 5, it is possible to observe a clear decrease of the cell parameters a and c , and an increase of the cell parameter b with increasing Eu content. This behaviour, as expected due to the nature of the substitution, is more pronounced in the unit cell volume which exhibits a decrease from $\sim 221 \text{ \AA}^3$ just above T_{MI} for NdNiO_3 to $\sim 220 \text{ \AA}^3$ in $\text{Nd}_{0.7}\text{Eu}_{0.3}\text{NiO}_3$. It is also observed that the Ni–O–Ni angle θ decreases and the Ni–O distance increases with increasing Eu substitution (figure 6).

Figures 4(a) and (b) show a small discontinuity of the cell parameters at temperatures where the MI transition takes place at ~ 200 and ~ 270 K for NdNiO_3 and $\text{Nd}_{0.7}\text{Eu}_{0.3}\text{NiO}_3$, respectively. The changes in the cell parameters b and c at T_{MI} were noticeable and accounted for $\sim 0.1\%$ and 0.06% , respectively. On the other hand, the observed change in the magnitude of the cell parameter a at T_{MI} was found to be smaller, yielding $\sim 0.03\%$.

These results are similar to those found in PrNiO_3 , NdNiO_3 , and SmNiO_3 by García-Muñoz *et al* [6], except for the case of the lattice parameter a in NdNiO_3 . They found a decrease in the lattice parameter a when the transition to the insulating phase takes place. Our results for this sample seems to be more accurate, and agree with those obtained by Lacorre *et al* [2] in samples of both PrNiO_3 and NdNiO_3 .

Within our experimental resolution, no vestiges of change in the crystal symmetry (orthorhombic, space group $Pbnm$) across the MI transition has been observed for both samples. This points to a kind of isomorphic transition, as frequently attributed to RNiO_3

Table 1. Structural parameters obtained via Rietveld analysis for the NdNiO₃ and Nd_{0.7}Eu_{0.3}NiO₃ compounds for three different temperatures. The average interatomic distances and the superexchange angle θ for the NiO₆ octahedra are also displayed.

Sample	NdNiO ₃			Nd _{0.7} Eu _{0.3} NiO ₃		
	170	214	301	230	280	300
a (Å)	5.395(1)	5.394(2)	5.399(2)	5.365(3)	5.362(3)	5.363(2)
b (Å)	5.383(1)	5.377(1)	5.380(1)	5.401(2)	5.398(2)	5.396(2)
c (Å)	7.616(2)	7.612(2)	7.617(2)	7.615(3)	7.612(3)	7.612(3)
V (Å ³)	221.16(1)	220.79(2)	221.25(2)	220.64(3)	220.32(3)	220.25(3)
R						
x	0.997(2)	0.998(2)	0.997(2)	0.993(2)	0.993(2)	0.993(2)
y	0.0370(6)	0.0349(7)	0.0345(7)	0.0400(1)	0.0397(1)	0.0388(1)
B (Å ²)	0.56(6)	0.14(6)	0.21(6)	0.30(8)	0.32(9)	0.34(9)
Ni						
B (Å ²)	0.15(4)	0.18(4)	0.22(4)	0.22(6)	0.26(6)	0.25(6)
O(1)						
x	0.076(2)	0.074(2)	0.075(2)	0.073(2)	0.072(2)	0.073(2)
y	0.490(1)	0.491(1)	0.491(1)	0.483(2)	0.484(2)	0.484(2)
B (Å ²)	0.12(3)	0.10(4)	0.12(8)	0.39(9)	0.42(9)	0.41(9)
O(2)						
x	0.715(1)	0.716(1)	0.715(1)	0.714(1)	0.714(1)	0.714(1)
y	0.289(1)	0.287(1)	0.286(1)	0.294(1)	0.294(1)	0.294(1)
z	0.0353(9)	0.0348(9)	0.0342(9)	0.0389(1)	0.0390(1)	0.0384(1)
B (Å ²)	0.41(6)	0.41(6)	0.53(8)	0.35(9)	0.38(9)	0.40(9)
$\langle \text{Ni–O}(1) \rangle$ (Å)	1.948(5)	1.945(5)	1.947(5)	1.945(5)	1.943(5)	1.943(5)
$\langle \text{Ni–O}(2) \rangle$ (Å)	1.945(5)	1.940(5)	1.942(5)	1.950(5)	1.949(5)	1.948(5)
$\langle \text{Ni–O} \rangle$ (Å)	1.946(5)	1.942(5)	1.944(5)	1.949(5)	1.947(5)	1.946(5)
$\langle \text{R–O} \rangle$ (Å)	2.521(5)	2.525(5)	2.528(5)	2.502(2)	2.503(2)	2.505(2)
θ (deg)	156.5(1)	157.0(1)	157.1(1)	155.2(2)	155.8(2)	155.6(2)
R_{Bragg}	2.8	2.9	3.0	6.0	5.4	5.7

(R = Nd and Pr) compounds at T_{MI} [6]. The absence of a change in the crystal symmetry across the MI transition in Nd-based nickelates is in agreement with recent Mössbauer spectroscopy data in NdNi_{0.98}Fe_{0.02}O₃ [18]. The authors could not find any evidence of more than one nickel chemical species, therefore indicating the absence of charge disproportionation in the light Fe-substituted NdNiO₃ compound. Such a result strongly suggests crystallographic equivalent Ni sites below T_{MI} in NdNiO₃.

Figure 5(a) exhibits a smooth thermal contraction of the unit cell volume with decreasing temperature for the NdNiO₃ compound. An abrupt and small increase of this value close to the MI transition temperature $T_{\text{ND}} \sim 193$ K ($\sim T_{\text{MI}}$) is also observed. Similar behaviour occurs for the Nd_{0.7}Eu_{0.3}NiO₃ sample, as seen in figure 5(b). In this case, the change in the unit cell volume takes place at $T_{\text{ND}} \sim 273$ K, a temperature similar to $T_{\text{MI}} \sim 270$ K obtained from the $\rho(T)$ data. The unit cell volume expansions were estimated to be $\Delta V/V_0 \sim 0.22\%$ and 0.18% for $x = 0$ and 0.30 , respectively. The result for $x = 0$ is in excellent agreement with the value of $\Delta V/V_0 = 0.23\%$ reported previously [6]. The value of $\Delta V/V_0 = 0.18\%$, for the sample with $x = 0.30$, is in line with the expected decrease of $\Delta V/V_0$ that is observed when the ionic radius is decreased.

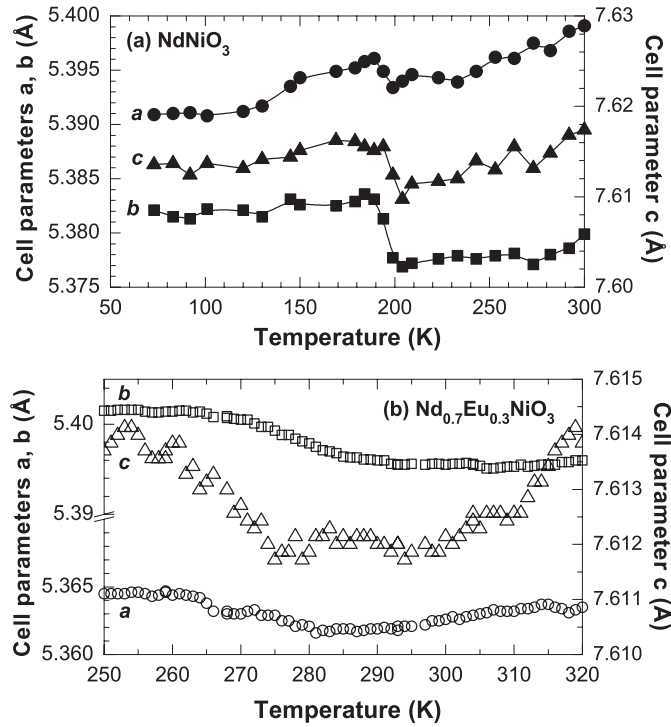


Figure 4. Temperature dependence of cell parameters a , b , and c for (a) NdNiO_3 and (b) $\text{Nd}_{0.7}\text{Eu}_{0.3}\text{NiO}_3$ showing the thermal expansion across the MI transition. The data were taken from NPD measurements upon warming.

The partial substitution of Nd by Eu also results in an appreciable change of the temperature width ΔT in which the MI transition occurs. This is clearly observed from the temperature dependence of the unit cell volume across the MI transition. From the data shown in figure 5, we have estimated $\Delta T \sim 15$ and 35 K for samples with $x = 0$ and 0.30, respectively. This remarkable difference in ΔT points to a change in the nature of the phase transition in this series.

Changes in the cell parameters and a small increase in the unit cell volume ($\Delta V/V_0 \sim 0.2\%$) when the insulating phase is established were detected. These changes are certainly related to the increase in the Ni–O bond length induced by electronic localization. The small change in the unit cell volume is in agreement with the ten-times smaller change of $\Delta V/V_0 \sim 0.02\%$ observed in BaVS_3 , a compound that undergoes an isomorphic MI transition [26]. On the other hand, the widely studied V_2O_3 system exhibits a much larger change in the unit cell volume at the MI transition ($\sim 3.5\%$), a feature that is accompanied by an actual change in the lattice symmetry from monoclinic to trigonal [27]. In the latter case, the MI transition seems to be more complicated, due to the role played by the structural changes in driving the MI transition. In any event, it seems that in the series studied here the relatively small changes in the unit cell volume are in fact induced by the electronic localization across the MI transition and not the driving mechanism for the transition.

Table 2 displays the thermal expansion coefficients α_L and α_V calculated for both samples above T_{MI} . The first one was estimated from the linear temperature dependence of the cell parameters a , b , and c above T_{MI} , and the α_V coefficients from the combined α_L values. These

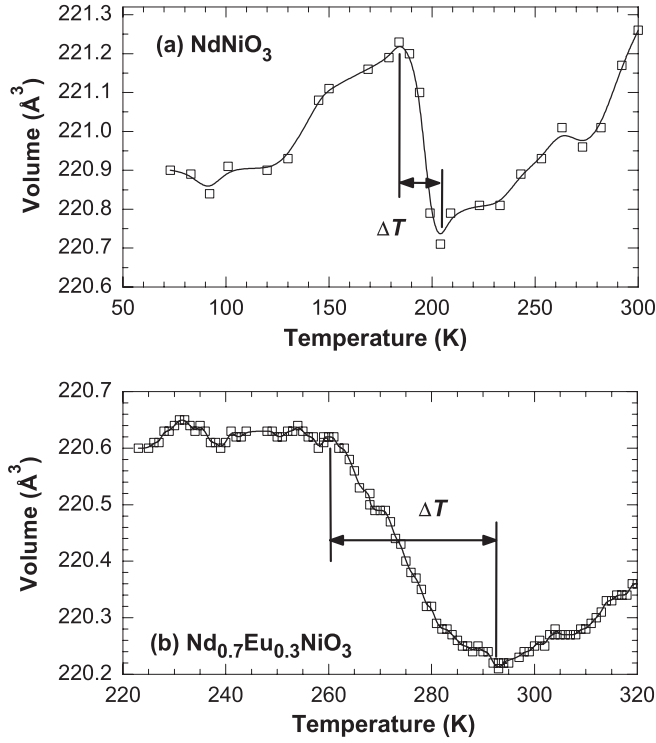


Figure 5. Temperature dependence of the unit cell volume V for (a) NdNiO_3 and (b) $\text{Nd}_{0.7}\text{Eu}_{0.3}\text{NiO}_3$. The data were taken from NPD measurements upon warming.

Table 2. Linear (α_L) and volumetric (α_V) thermal expansion coefficients calculated for the metallic phase in both compounds: NdNiO_3 ($x = 0$) and $\text{Nd}_{0.7}\text{Eu}_{0.3}\text{NiO}_3$ ($x = 0.30$).

x	α_L^a (10^{-6}) K^{-1}	α_L^b (10^{-6}) K^{-1}	α_L^c (10^{-6}) K^{-1}	α_V (10^{-5}) K^{-1}
0	13.2	4.3	8.8	2.62
0.30	14.7	1.8	12.9	2.48

coefficients were also obtained for the insulating phase (not shown) in a similar fashion. The thermal expansion coefficient related to the cell parameter b , α_L^b , was found to exhibit the smallest overall thermal expansion, but the largest discontinuity at the phase transition. These results seem to be in good agreement with those already obtained by García-Muñoz *et al* [6] in both PrNiO_3 and SmNiO_3 . In addition, increasing Eu content resulted in an increase of both α_L^a and α_L^c values and a decrease of α_L^b . It is well known that the variation of structural parameters could be a response to the subtle change in the structural arrangement [6]. In fact, the expansion of the unit cell at T_{MI} , when the system evolves to the insulating state, is accompanied by at least two major changes in the unit cell parameters: an increase of the average Ni–O distance $d_{\text{Ni–O}}$, and a decrease of the Ni–O–Ni bond-angle θ .

The average Ni–O distance ($d_{\text{Ni–O}}$) and the superexchange angle (θ) were thus calculated in order to verify the structural changes across the MI transition for the two samples analysed. The temperature dependence of $d_{\text{Ni–O}}$ and θ obtained for both samples are depicted in figure 6. The temperature dependence of $d_{\text{Ni–O}}$ across the MI transition exhibits similar behaviour for

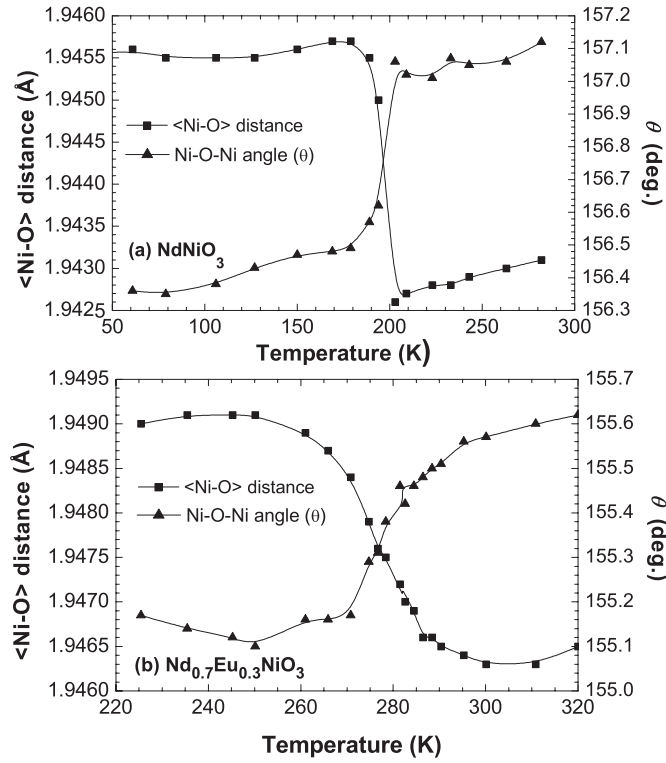


Figure 6. Average Ni–O distance ($\langle\text{Ni–O}\rangle$) and Ni–O–Ni superexchange angle (θ) for samples of (a) NdNiO_3 and (b) $\text{Nd}_{0.7}\text{Eu}_{0.3}\text{NiO}_3$ obtained from Rietveld refinements of the NPD data.

both compounds. A small expansion of $d_{\text{Ni–O}}$ at T_{MI} was verified when the temperature is decreased. The changes in the $\langle\text{Ni–O}\rangle$ distance were estimated to be $\Delta d_{\text{Ni–O}} \sim 0.003$ Å for both compounds, a value comparable to those found in NdNiO_3 and PrNiO_3 [6]. However, it is worth mentioning that the change in $d_{\text{Ni–O}}$ at T_{MI} for the sample with $x = 0$ is much sharper in temperature than for the sample with $x = 0.30$. The $\langle\text{Ni–O}\rangle$ distance has been estimated to be $d_{\text{Ni–O}} \sim 1.94$ Å, a value that is in excellent agreement with previous results for NdNiO_3 [6].

The temperature dependence of the superexchange angle θ also exhibits a smooth contraction $\Delta\theta$ close to T_{MI} with decreasing temperature, as usually observed in other nickelates [2, 3]. An estimate of this angular change at T_{MI} yielded values of $\Delta\theta \sim -0.5^\circ$ and -0.4° for the samples of NdNiO_3 and $\text{Nd}_{0.7}\text{Eu}_{0.3}\text{NiO}_3$, respectively. However, these changes in $\Delta\theta$ across the MI transition can be estimated by considering that such a change is due solely to steric effects, or more appropriately, to the decrease of the average Ni–O distance at T_{MI} [6].

Within this context, it is possible to relate the degree of distortion of the ideal perovskite structure, characterized by the tolerance factor t , along with the superexchange angle θ . The tolerance factor is defined as

$$t = \frac{d_{\text{R–O}}}{d_{\text{Ni–O}}\sqrt{2}} \quad (1)$$

where $d_{\text{R–O}}$ is the average (Nd/Eu)–O distance and $d_{\text{Ni–O}}$ is the average Ni–O distance. Therefore, a linear approximation which correlates θ and t resulted in $\theta \sim 267.3t$. Differentiating this relation and the expression for the tolerance factor, and combining both

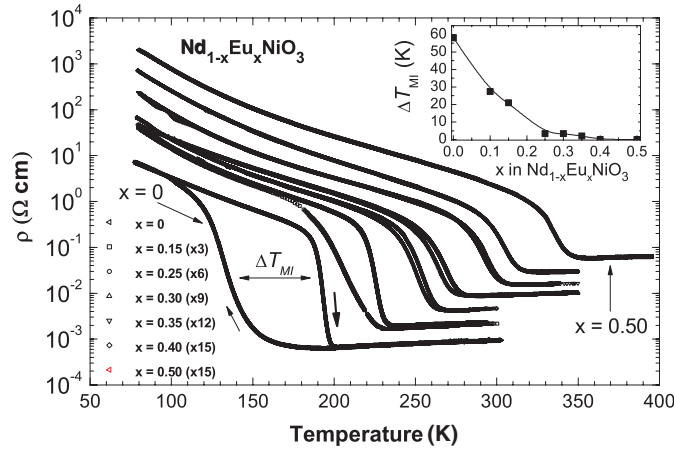


Figure 7. Temperature dependence of electrical resistivity $\rho(T)$ of $\text{Nd}_{1-x}\text{Eu}_x\text{NiO}_3$ ($0 \leq x \leq 0.5$) compounds. The data were taken during the heating and the cooling processes, as indicated by the arrows. The inset displays the ΔT_{MI} against x curve.

results, the expected variation of the θ angle ($\Delta\theta$) across the MI transition is given by

$$\Delta\theta = -267.3 \frac{d_{\text{R-O}}}{d_{\text{Ni-O}}^2 \sqrt{2}} \Delta d_{\text{Ni-O}} \quad (2)$$

where $\Delta d_{\text{Ni-O}}$ is the variation of $d_{\text{Ni-O}}$ at temperatures close to T_{MI} .

By using such an approximation, $\Delta\theta$ values of $\sim -0.38^\circ$ and -0.32° were estimated for the samples with $x = 0$ and 0.30 , respectively. The very good agreement between the measured and estimated values of $\Delta\theta$ indicates that the expansion in the structural and geometrical parameters could be understood as a steric response to the increase of the Ni–O distance caused by the electronic localization occurring at T_{MI} . The values obtained here for both samples were slightly smaller than $\Delta\theta \approx -0.46^\circ$ obtained before for NdNiO_3 [6], but with the same sign and the same order of magnitude.

3.2. Electrical resistivity

The most striking feature displayed by this series is the occurrence of a metal–insulator (MI) transition in a wide range of temperature. Such a transition is easily seen in the temperature dependence of the electrical resistivity, $\rho(T)$, for the samples of $\text{Nd}_{1-x}\text{Eu}_x\text{NiO}_3$ ($0 \leq x \leq 0.5$), as shown in figure 7. The overall behaviour of the $\rho(T)$ data is essentially the same for all samples and they exhibit four important features: (1) a continuous increase in the MI transition temperature with increasing Eu content; (2) a metallic-like behaviour above T_{MI} , with a linear temperature dependence of $\rho(T)$; (3) a fairly rapid increase of $\rho(T)$ at T_{MI} , related to the temperature-driven MI transition; and (4) a clear thermal hysteresis occurring in a temperature interval ΔT_{MI} close to T_{MI} , which decreases appreciably as T_{MI} increases.

The temperature in which the MI transition occurs is rather sensitive to Eu concentration, as can be inferred from the data of figure 7. The $\rho(T)$ data reveal that T_{MI} increases continuously with increasing Eu concentration, ranging from ~ 193 K in NdNiO_3 to 336 K in $\text{Nd}_{0.5}\text{Eu}_{0.5}\text{NiO}_3$ sample. The computed T_{MI} values are displayed in table 3. The NdNiO_3 sample was found to exhibit $T_{\text{MI}} \sim 193$ K, a value in excellent agreement with others listed in the literature [10]. Increasing Eu content resulted in a systematic increase of T_{MI} , a behaviour consistent with

Table 3. Values of T_{MI} , ρ_0 , A , λ_{tr} and l for $\text{Nd}_{1-x}\text{Eu}_x\text{NiO}_3$. T_{MI} was obtained from $(1/\rho)(d\rho/dT)$ against T curves, and ρ_0 and A were obtained through the linear fitting of the experimental data in the metallic regime. The mean free path l values were estimated for a temperature just above the MI transition.

x	T_{MI} (K)	ρ_0 ($10^{-4} \Omega \text{ cm}$)	A ($10^{-6} \Omega \text{ cm K}^{-1}$)	λ_{tr}	l (\AA)
0	193	0.82	1.70	0.42	16.0
0.10	215	1.04	1.30	0.32	19.7
0.15	226	0.97	2.32	0.57	18.8
0.25	254	1.47	1.37	0.34	12.9
0.30	270	3.28	2.45	0.60	10.8
0.35	293	4.76	2.59	0.64	8.4
0.40	304	7.88	3.54	0.87	5.5
0.50	336	20.2	5.42	1.33	2.8

intermediary values of T_{MI} ranging between $T_{\text{MI}} \sim 196 \text{ K}$ for NdNiO_3 and $T_{\text{MI}} \sim 480 \text{ K}$ for EuNiO_3 [10].

The $\rho(T)$ data in the metallic regime, $T > T_{\text{MI}}$, was described as $\rho(T) = \rho_0 + AT$ for all samples studied. Such a behaviour of $\rho(T)$ is typical of electron–phonon scattering where ρ_0 is the residual electrical resistivity and A is related to the electron–phonon coupling constant λ_{tr} . Assuming that the linear dependence of the electrical resistivity is due entirely to electron–phonon scattering, then λ_{tr} can be obtained by using [28]

$$\lambda_{\text{tr}} = 0.246(\hbar\omega_{\text{p}})^2 A. \quad (3)$$

Considering the plasmon energy $\hbar\omega_{\text{p}} \approx 1 \text{ eV}$, the same value obtained for LaNiO_3 [29], then λ_{tr} can be estimated for all samples. It is also possible to estimate the mean free path l from

$$l = \frac{4.95 \times 10^{-4} v_{\text{F}}}{(\hbar\omega_{\text{p}})^2 \rho} \quad (4)$$

where v_{F} (the Fermi velocity) was assumed to be of the same magnitude as that similar oxides ($v_{\text{F}} \sim 2.2 \times 10^{-4} \text{ cm s}^{-1}$ for $\text{La}_{1.825}\text{Sr}_{0.175}\text{CuO}_4$) [30].

From fits of $\rho(T)$ data we have obtained increasing values of both ρ_0 and A with increasing Eu content. All these values, as well as the values of λ_{tr} , and l for all samples, are summarized in table 3. The mean free path l was estimated for a temperature just above the transition temperature T_{MI} . The values of ρ_0 and A are of the same magnitude as those found in other related nickelates such as, for instance, $\rho_0 = 4.6 \times 10^{-4} \Omega \text{ cm}$ and $A = 2.7 \times 10^{-6} \Omega \text{ cm K}^{-1}$ obtained in SmNiO_3 [8]. It is important to mention that the values of ρ_0 are expected to be dependent on the heat treatments during the sample preparation as well as on the oxygen nonstoichiometry [22, 31].

Just below T_{MI} , the electrical resistivity jumps by three or four orders of magnitude and the electrical resistivity of the system is better described by an Arrhenius-type activation process $\rho(T) = \rho_{\text{s}} \exp(E_{\text{g}}/k_{\text{B}}T)$, where ρ_{s} is the temperature-independent electrical resistivity, E_{g} is the energy gap, and k_{B} is the Boltzmann constant. We have fitted the low-temperature data and obtained the activation energy $E_{\text{g}} \sim 44$ and 73 meV for NdNiO_3 and $\text{Nd}_{0.7}\text{Eu}_{0.3}\text{NiO}_3$ compounds, respectively. The activation energy is similar to that obtained by Granados *et al* [32] (25–28 meV) in the same compound with $x = 0$, although their results showed a smooth curvature in the $\lg R$ against $1/T$ curves, indicating that a simple activated behaviour is only a rough approximation of the insulating phase. There are indications that the activation energy

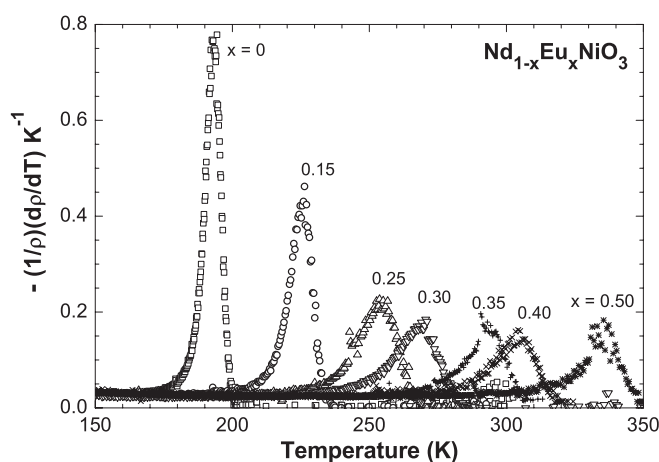


Figure 8. Temperature dependence of $(1/\rho)(d\rho/dT)$, obtained during the heating process.

is also strongly dependent on the preparation process, since a small oxygen nonstoichiometry deeply affects the behaviour of the insulating phase [31].

Examining the $\rho(T)$ curves in figure 7 further, one can note that the thermal hysteresis ΔT_{MI} is noticeable only in samples with $x < 0.30$. In fact, it occurs in a temperature interval ΔT_{MI} as large as 58 K in NdNiO_3 and is much less pronounced, or nearly absent, for the compound $\text{Nd}_{0.65}\text{Eu}_{0.35}\text{NiO}_3$, where $\Delta T_{\text{MI}} \sim 2$ K (see the inset of figure 7). The hysteretic behaviour observed here, at least for the parent compound, is certainly related to the first-order character of the MI transition and reflects the temperature interval ΔT_{MI} in which both phases, metallic (disordered) and insulating (ordered), coexist [11, 19]. The ΔT_{MI} against x plot shown in the inset of figure 7 also indicates that the width ΔT_{MI} of this thermal hysteresis approaches zero for Eu content $x \sim 0.25$. This strongly suggests that the partial substitution of Nd by Eu modifies the character of this transition from first to second order in samples with Eu content higher than ~ 0.25 . Similar behaviour has been observed in $\text{Nd}_{0.5}\text{Sm}_{0.5}\text{NiO}_3$ which exhibited absence of thermal hysteresis in $\rho(T)$ measurements, and the MI transition was characterized as a second-order phase transition [21]. This proposition has to be further explored since a decrease in ΔT_{MI} is also expected as T_{MI} increases.

It should be mentioned that Nikulin *et al* [31] could not observe any noticeable thermal hysteresis in electrical resistivity measurements performed in SmNiO_3 . This behaviour was explained as a result of the kinetics of the MI phase transition, since the phase transition for SmNiO_3 occurs at temperatures much higher than that for NdNiO_3 . The kinetics of the phase transformation is believed to be much slower for the compound with Nd than that for the compound with Sm, resulting in a noticeable thermal hysteresis only for the NdNiO_3 compound.

Figure 8 shows the temperature dependence of the logarithmic derivative of the electrical resistivity curves, $(1/\rho)(d\rho/dT)$ against T , taken upon heating. The peaks provide a better means of defining the value of T_{MI} , as opposed to the simple inspection of the $\rho(T)$ curves [33]. The MI transition is sharper for the parent compound, a feature that manifests itself in the width of the peak in $(1/\rho)(d\rho/dT)$.

The broadening and the decrease of the peak intensity in $(1/\rho)(d\rho/dT)$ with increasing Eu content suggest a continuous transition from the metallic to the insulating state. In addition, the trend shown in figure 8 indicates that increasing substitution of Nd by Eu in NdNiO_3 moves the transition away from a well defined value of T_{MI} . This behaviour is certainly related to the increase of disorder which is also responsible for the observed increase in the value of ρ_0 with

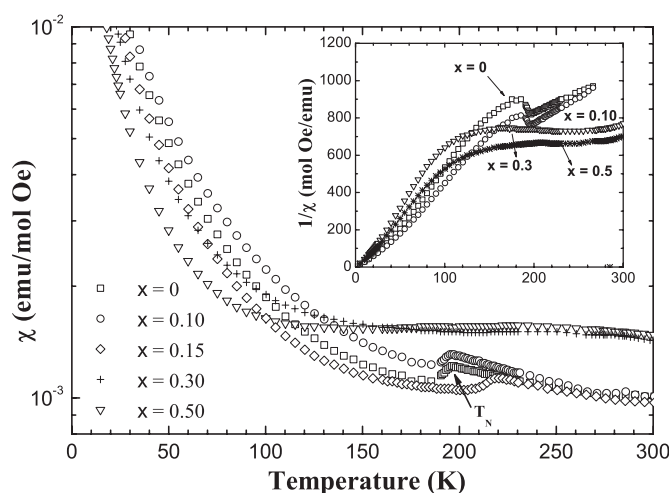


Figure 9. Curves of $\chi(T)$ for $\text{Nd}_{1-x}\text{Eu}_x\text{NiO}_3$ ($0 \leq x \leq 0.5$) after the subtraction of the contribution of the rare-earth ions. The inset shows the $1/\chi(T)$ curves.

increasing Eu content (see table 3). Such a partial substitution is analogous to an increase of the quenched bond randomness observed in systems such as LaMnO_3 [34]. In other words, the coexistence between the ordered and disordered phases at the phase transition disappears at a finite threshold amount of Eu. In fact, neutron diffraction data have also suggested an increase of the crystalline disorder in the $\text{Nd}_{0.7}\text{Eu}_{0.3}\text{NiO}_3$ sample, as inferred from the temperature interval in which the MI transition occurs (see figures 5 and 6).

3.3. Magnetization

Magnetization measurements $M(T)$ were performed in all samples of $\text{Nd}_{1-x}\text{Eu}_x\text{NiO}_3$ under magnetic fields H up to 10 kOe. The magnetic susceptibility $\chi(T)$ was obtained from $\chi(T) = M(T)M_m/Hm$, where M_m is the molecular mass and m is the mass of the sample.

In order to understand the magnetic behaviour of these systems better, specifically the behaviour of the Ni sublattice which orders antiferromagnetically, the magnetic contribution of the rare-earth ions to the susceptibility $\chi(T)$ was subtracted from the original data. This subtraction was performed through measurements of magnetization in samples with similar crystal structure but without evidence for magnetic ordering of the metal. In this case, samples of NdAlO_3 and EuAlO_3 were prepared, in which the Ni ion was fully replaced by Al.

Once the corresponding $\chi(T)$ curves for the Al substituted samples were obtained, they were fitted to a Curie–Weiss law in the high-temperature region ($T > 100$ K). Hence, it was possible to obtain the magnetic susceptibility for each ion separately (Nd^{3+} and Eu^{3+}). Finally, the contribution of the Ni ions (Ni^{3+}) to the total observed susceptibility $\chi(T)$ could be written as

$$\chi^{\text{Ni}^{3+}} = \chi(T) - \chi^{\text{Nd}^{3+}}(1-x) - \chi^{\text{Eu}^{3+}}(x). \quad (5)$$

Figure 9 displays a typical set of $\chi(T)$ curves after performing the subtraction discussed above. The data belonging to the samples with $x = 0, 0.10$, and 0.15 display a clear peak near ~ 200 K, corresponding to the antiferromagnetic ordering of the Ni^{3+} sublattice. For samples with $x = 0$ and $x = 0.10$, $T_N \sim 195$ K and for $x = 0.15$, $T_N \sim 220$ K.

The $\chi(T)$ curves for the samples where T_N is well defined ($x = 0$, $x = 0.10$ and $x = 0.15$) were fitted by the form $\chi(T) = \chi_0 + C/(T - \theta_c)$, where C is the Curie constant, θ_c is the Curie–Weiss temperature and χ_0 is a temperature-independent contribution to the susceptibility. By using the Curie constant C obtained in these fits, the values obtained for μ_{eff} were 1.75, 1.73, and 1.79 μ_B for the samples with $x = 0$, 0.10, and 0.15 respectively. These values are in excellent agreement with $\mu_{\text{eff}} \sim 1.76\mu_B$ expected for the free Ni³⁺ ion at $T > T_N$.

The expected peak of the magnetic order of the Ni sublattice is hardly seen in curves from samples with $x \geq 0.3$. This might be explained by the fact that increasing Nd substitution by Eu results in a stronger effect of the crystalline electric field (CEF). Therefore, higher values of $\chi(T)$ are obtained, hiding the observation of the magnetic order of the Ni sublattice. Besides, the magnetic contribution of the CEF of the Eu³⁺ is bigger than that of Nd³⁺ ions, which makes the separation of the Ni sublattice contribution more difficult than the one performed above.

The magnitude of χ increases monotonically when the temperature is decreased below T_N . This indicates that the thermal behaviour of the Ni sublattice cannot be understood within the framework of a conventional antiferromagnet. One possible explanation for this anomalous behaviour would be the presence of a canted-spin ferromagnetism. In fact, a small irreversibility observed in our measurements in ZFC and FC curves (not shown) would be an indication of weak ferromagnetism. However, the irreversibility was observed to be almost field independent, which seems to be inconsistent with the canted-spin picture.

On the other hand, the low-temperature behaviour of the magnetic susceptibility could be a result of two magnetic phases that coexist below T_N : one antiferromagnetic phase, where the magnetic susceptibility decreases when the temperature decreases, and a paramagnetic phase, where the magnetic susceptibility increases further when the temperature decreases. This anomalous behaviour in the magnetic susceptibility has been reported previously by Zhou *et al* [35] in measurements performed in NdNiO₃ and Nd_{0.5}Sm_{0.5}NiO₃ and was attributed to a charge disproportionation in the Ni sublattice, resulting in alternating diamagnetic and paramagnetic Ni sites. This point needs to be better clarified, and experiments are under way to address that.

4. Conclusions

In summary, we have produced high-quality polycrystalline samples of Nd_{1-x}Eu_xNiO₃ ($0 \leq x \leq 0.5$). From XRD and NPD results we have found single-phase samples that crystallize in the GdFeO₃-type orthorhombically distorted perovskite structure (space group *Pbnm*). The thermal evolution of the structural parameters across the MI transition revealed small unit cell changes at temperatures close to the MI transition. Within our experimental resolution, it was not possible to observe any kind of structural phase transition at T_{MI} through the analysis of the NPD data. The MI transition temperatures from NPD measurements (T_{ND}) were in good agreement with those found through electrical resistivity (T_{MI}) measurements.

The magnetic susceptibility data indicate, after subtracting the magnetic contribution of the rare-earth ions, that χ increases below T_N for all samples, suggesting a possible coexistence of two phases: a paramagnetic phase and an antiferromagnetic one. However, this point still needs to be better clarified.

The substitution of Nd by Eu in the NdNiO₃ compound causes a broadening in the variation of the unit cell volume across the MI transition, which is also reflected in both the temperature dependence of the Ni–O distance and the superexchange angle. An increase of ρ_0 in the electrical resistivity curves is also observed, as the Eu content increases, and the transition becomes less defined. When the Eu content is higher than ~ 0.25 , the thermal hysteresis observed in the electrical resistivity curves, between the heating and cooling process, is suppressed. These results indicate that crystalline disorder, induced by the progressive

substitution of Nd by Eu, is changing the first-order character of the phase transition observed across the MI boundary.

Acknowledgments

The authors have benefited from the technical assistance of Walter Soares de Lima. This work was supported by the Brazilian agency Fundação de Amparo à Pesquisa do Estado de São Paulo (FAPESP) under Grant No 05/53241-9. One of us (MTE) acknowledges a FAPESP fellowship under Grant No 97/11369-0 and RFJ the Conselho Nacional de Desenvolvimento Científico e Tecnológico (CNPq) fellowship under Grant No 303272/2004-0. The Institut Laue-Langevin (Grenoble) is acknowledged for the allocated beam time on the D20 diffractometer.

References

- [1] Bednorz J G and Müller K A 1986 *Z. Phys.* B **64** 189
- [2] Lacorre P, Torrance J B, Pannetier J, Nazzari A I, Wang P W and Huang T C 1991 *J. Solid State Chem.* **91** 225
- [3] Torrance J B, Lacorre P, Nazzari A I, Ansaldo E J and Niedermayer C 1992 *Phys. Rev. B* **45** 8209
- [4] Xu X Q, Peng J L, Li Z Y, Ju H L and Greene R L 1993 *Phys. Rev. B* **48** 112
- [5] García-Muñoz J L, Rodríguez-Carvajal J and Lacorre P 1992 *Europhys. Lett.* **20** 241
- [6] García-Muñoz J L, Rodríguez-Carvajal J, Lacorre P and Torrance J B 1992 *Phys. Rev. B* **46** 4414
- [7] Escote M T 2002 *PhD Thesis* Instituto de Física, Universidade de São Paulo, Brazil
- [8] Pérez-Cacho J, Blasco J, García J, Castro M and Stankiewicz J 1999 *J. Phys.: Condens. Matter* **11** 405
- [9] Vobornik I, Perfetti L, Zacchigna M, Grioni M, Margaritondo G, Mesot J, Medarde M and Lacorre P 1999 *Phys. Rev. B* **60** R8426
- [10] Medarde M, Lacorre P, Conder K, Rodríguez-Carvajal J, Rosenkranz S, Fauth F and Furrer A 1998 *Physica B* **241–243** 751
- [11] Medarde M L 1997 *J. Phys.: Condens. Matter* **9** 1679 and references therein
- [12] Alonso J A, García-Muñoz J L, Fernández-Díaz M T, Aranda M A G, Martínez-Lope M J and Casais M T 1999 *Phys. Rev. Lett.* **82** 3871
- [13] Alonso J A, Martínez-Lope M J, Casais M T, García-Muñoz J L, Fernández-Díaz M T and Aranda M A G 2001 *Phys. Rev. B* **64** 94102
- [14] Zhou J-S, Goodenough J B and Dabrowski B 2004 *Phys. Rev. B* **70** 81102(R)
- [15] Escote M T and Jardim R F 2001 *J. Magn. Magn. Mater.* **226** 249
- [16] Zaghrioui M, Bulou A, Lacorre P and Laffez P 2001 *Phys. Rev. B* **64** 81102
- [17] Staub U, Meijer G I, Fauth F, Allenspach R, Bednorz J G, Karpinski J, Kazakov S M, Paolasini L and d'Acapito F 2002 *Phys. Rev. Lett.* **88** 126402
- [18] Presniakov I, Demazeau G, Baranov A, Sobolev A and Pokholok K 2005 *Phys. Rev. B* **71** 054409
- [19] García-Muñoz J L, Rodríguez-Carvajal J and Lacorre P 1994 *Phys. Rev. B* **50** 978
- [20] García-Muñoz J L, Lacorre P and Cywinski R 1995 *Phys. Rev. B* **51** 15197
- [21] Zhou J-S, Goodenough J B, Dabrowski B, Klamut P W and Bukowski Z 2000 *Phys. Rev. B* **61** 4401
- [22] Escote M T, da Silva A M L, Matos J R and Jardim R F 2000 *J. Solid State Chem.* **151** 298
Escote M T and Jardim R F 1998 *Radiat. Eff. Defects Solids* **147** 101
- [23] Rodríguez-Carvajal J 1993 *Physica B* **192** 55
- [24] Demazeau G, Marbeuf A, Pochard M and Hagenmuller P 1971 *J. Solid State Chem.* **13** 582
- [25] Alonso J A, Martínez-Lope M J and Rasines I 1995 *J. Solid State Chem.* **120** 170
- [26] Graf T, Mandrus D, Lawrence J M, Thompson J D, Canfield P C, Cheong S-W and Rupp L W Jr 1995 *Phys. Rev. B* **51** 2037
- [27] Goodenough J B 1992 *Phys. Rev. B* **45** 8209
- [28] Escote M T, Meza V A, Jardim R F, Ben-Dor L, Torikachvili M S and Lacerda A H 2002 *Phys. Rev. B* **66** 144503
- [29] Kemp J P and Cox P A 1990 *Solid State Commun.* **75** 731
- [30] Gurvitch M and Fiory A T 1987 *Phys. Rev. Lett.* **59** 1337
- [31] Nikulin I V, Novojilov M A, Kaul A R, Mudretsova S N and Kondrashov S V 2004 *Mater. Res. Bull.* **39** 775
- [32] Granados X, Fontcuberta J, Obradors X, Mañosa L and Torrance J B 1993 *Phys. Rev. B* **46** 11666
- [33] Fisher M E and Langer J S 1968 *Phys. Rev. Lett.* **20** 665
- [34] Dagotto E, Hotta T and Moreo A 2001 *Phys. Rep.* **344** 1
- [35] Zhou J-S, Goodenough J B, Dabrowski B, Klamut P W and Bukowski Z 2000 *Phys. Rev. Lett.* **84** 526